Geometrically disordered network models, quenched quantum gravity, and critical behavior at quantum Hall plateau transitions

I. A. Gruzberg, A. Klümper, W. Nuding, and A. Sedrakyan

Phys. Rev. B **95**, 125414 — Published 10 March 2017

DOI: 10.1103/PhysRevB.95.125414

Geometrically disordered network models, quenched quantum gravity, and critical behavior at quantum Hall plateau transitions

I. A. Gruzberg
Ohio State University, Department of Physics, 191 W. Woodruff Ave, Columbus OH, 43210

A. Klümper and W. Nuding
Bergische Universität Wuppertal, Gaußstraße 20, 42119 Wuppertal, Germany

A. Sedrakyan
Yerevan Physics Institute, Br. Alikhanian 2, Yerevan 36, Armenia
(Dated: February 12, 2017)

Recent results for the critical exponent of the localization length at the integer quantum Hall transition differ considerably between experimental ($\nu_{\rm exp} \approx 2.38$) and numerical ($\nu_{\rm CC} \approx 2.6$) values obtained in simulations of the Chalker-Coddington (CC) network model. The difference is at least partially due to effects of the electron-electron interaction present in experiments. Here we propose a mechanism that changes the value of ν even within the single-particle picture. We revisit the arguments leading to the CC model and consider more general networks with structural disorder. Numerical simulations of the new model lead to the value $\nu \approx 2.37$. We argue that in a continuum limit the structurally disordered model maps to free Dirac fermions coupled to various random potentials (similar to the CC model) but also to quenched two-dimensional quantum gravity. This explains the possible reason for the considerable difference between critical exponents for the CC model and the structurally disordered model. We extend our results to network models in other symmetry classes.

PACS numbers: 73.43.-f; 71.30.+h;72.15.Rn; 73.20.Fz

I. INTRODUCTION

The integer quantum Hall (QH) transition[1] is the most prominent example of an Anderson transition, a quantum phase transition driven by disorder and accompanied by universal critical phenomena.[2] Many experiments[3–9] demonstrated scaling near the integer QH transition characterized by the product of the localization length exponent ν and a dynamical exponent z. Ref. [10] reported a direct measurement of the dynamical exponent $z = 1$ using samples of different sizes. This result remains controversial, see a discussion in Ref. [11]. However, if we assume $z = 1$, then the experimental value of ν turns out to be $\nu_{\rm exp} = 2.38 \pm 0.02$.[10] A similar value of νz was observed at the integer QH transition in graphene.[12]

The integer QH transition is usually modeled within the paradigm of Anderson localization,[13,14] neglecting electron-electron interactions. Existence of delocalized states in disorder-broadened Landau levels, which is necessary to explain the integer QH transition, is consistent with the description of the transition by a nonlinear sigma model[15,16] and its two-parameter flow diagram.[17,18] The critical point of the sigma model should possess conformal invariance and be described by a conformal field theory (CFT) with the central charge $c = 0$.[19] However, this fixed point is in the strong coupling regime, and notable attempts at identifying the CFT[20–23] are inconclusive so far.

The integer QH transition is related to the model of Dirac fermions with random mass, scalar, and gauge potentials.[24] A simplified model with a random gauge potential only is analytically solvable, and the exact spectrum of multifractal exponents describing the scaling of the moments of critical wave functions is known.[24–30]

Alternative approaches to the integer QH transition were recently advanced. One employs a mapping to a classical model and conformal restriction.[31] Another uses symmetries of the sigma model[32,33] to derive exact properties of the multifractal spectra at the integer QH transition. Still another approach allows a direct microscopic construction of scaling operators is the network model (see below).[34] Combined with some general features of CFTs this approach leads to a prediction of an exactly parabolic multifractal spectrum.[35] In spite of these successes, no theoretical predictions for the exponent ν exist.

Much intuition about the integer QH transition, as well as the most accurate numerical estimates for critical exponents, come from the Chalker-Coddington (CC) network model.[36,37] The model is based on the semiclassical picture of electrons drifting along the equipotential lines of the disorder potential and tunneling across saddle points. In the CC model this picture is drastically simplified: all saddle points are represented by scattering matrices at the vertices of a square lattice. The CC model can be mapped both to the nonlinear sigma model[38,39] and to random Dirac fermions.[40]

The regular geometry of the CC model allows one to apply numerical transfer matrix techniques.[41,42] Recent implementations of this[43–48] and other methods[49,50] agree on the value ν in the range 2.56–2.62, certainly different from $\nu_{\rm exp}$. The discrepancy points to the importance of the long-range electron-electron interaction,

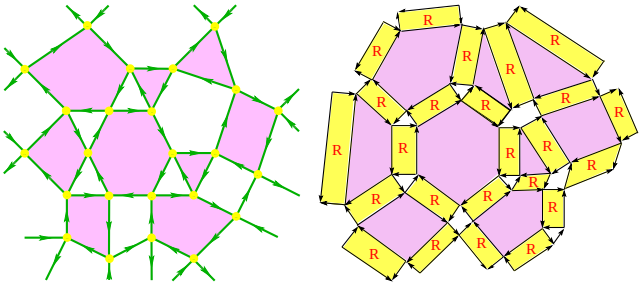

Figure 1. Left: a random graph. Right: the corresponding random medial lattice.

which certainly affects the scaling near the integer QH transition[51–58] and is relevant for the interpretation of experiments.

In this paper we focus on a mechanism that leads to a modification of ν from its CC value even within the single-particle framework. Namely, we propose that the CC model does not capture all types of disorder that are relevant at the integer QH transition. Indeed, saddle points that connect the "puddles" of filled electron states do not form a regular lattice, and around each "puddle" there may be any number of them. Taking this into account leads us to consider structurally disordered, or *random networks* that better represent the physics in a smooth disorder potential and strong magnetic field.

Let us list the main results of this paper.

(1) An ensemble of random networks can be mapped in a continuum limit to the problem of Dirac fermions coupled to random potentials (similar to the CC model) and also to two-dimensional (2D) quantum gravity. Coupling to 2D quantum gravity modifies critical exponents of statistical mechanics models.[59–65] We suggest that a similar modification happens for random networks.

(2) Random networks can be effectively constructed starting with the CC network and appropriately modifying it. These random networks can then be numerically simulated, and for certain values of parameters specifying the geometric disorder, we obtain the localization length exponent $\nu = 2.372 \pm 0.017$, in surprising (and most likely, acidental) agreement with experiments.

(3) We extend these ideas to QH transitions in symmetry classes C and D in the classification of Refs. [66, 67]. Properties of these transitions map to classical statistical mechanics models which were studied on random lattices, and for which the shift in critical exponents is given by the Knizhnik-Polyakov-Zamolodchikov (KPZ) relation[59–61] from the theory of 2D quantum gravity. This fact allows us to predict various exact critical exponents for these transitions.

II. RANDOM NETWORKS

The network models we consider are built on planar directed graphs where every vertex has two incoming and two outgoing edges. The in- and out- edges, also called

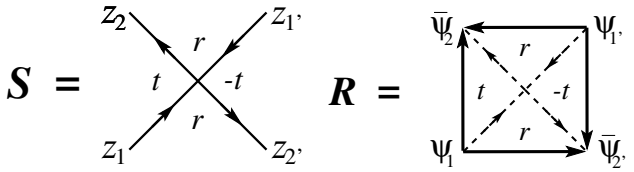

Figure 2. Left: an S matrix. Right: the corresponding R matrix.

links of the network, alternate as one goes around a vertex. Such graphs divide the plane into two sets of polygonal faces with opposite orientations of their edges, see Fig. 1, left. These are exactly the Feynman graphs of a zero-dimensional (complex) matrix ϕ^4 theory in the large N limit.[68,69]

A state of the network model on a given random graph is represented by a complex vector $Z \in \mathbb{C}^N$, where N is the number of edges of the graph, and each component z_e corresponds to the complex flux on the edge e. The model includes random scattering matrices connecting incoming $z_1, z_{1'}$ and outgoing $z_2, z_{2'}$ fluxes (see Fig. 2):

$$\begin{pmatrix} z_2 \\ z_{2'} \end{pmatrix} = \mathcal{S} \begin{pmatrix} z_1 \\ z_{1'} \end{pmatrix} = \begin{pmatrix} te^{i\gamma} & re^{i\gamma'} \\ re^{i\gamma} & -te^{i\gamma'} \end{pmatrix} \begin{pmatrix} z_1 \\ z_{1'} \end{pmatrix}, \qquad (1)$$

placed at the vertices. The scattering amplitudes satisfy $t^2 + r^2 = 1$, and the scattering phases γ, γ' are random.

Evolution of the network in discrete time steps is specified by an $N \times N$ unitary matrix U composed of all node scattering matrices.[70] In this description the basic object is the resolvent $(1 - e^{-\eta} U)^{-1}$. Its matrix element (a Green function) can be written as a superintegral

$$G(e_1, e_2; \eta) = \int \mathcal{D}\Psi \, \psi_{e_1} \bar{\psi}_{e_2} e^{-\sum_{e,e'} \bar{\Psi}_e (1 - e^{-\eta} U)_{ee'} \Psi_{e'}} \qquad (2)$$

where e_1, etc., label edges of the graph, and $\bar{\Psi}_e = (\bar{\phi}_e, \bar{\psi}_e)$ consists of bosonic (ϕ) and fermionic (ψ) variables assigned to the edge e. The use of bosonic and fermionic variables is standard in the supersymmetry method, and is necessary to perform disorder averages, see Refs. [71, 72] for details. For our purposes it is sufficient to take $\eta = 0$ in what follows.

Random networks were recast as lattice models in Ref. [73] in connection with the string representation of the 3D Ising model, and further studied in Refs. [74–78]. Following these works, we connect the midpoint of each edge e "forward" to two other midpoints by two vectors ξ_e. These vectors together form the *medial lattice* of the original random network. Then a scattering node is replaced by a rectangle (Fig. 2), and we get an alternative representation of the random network as a random medial lattice (Fig. 1). The action for the random network written as

$$S = \sum_e \bar{\Psi}_e \Psi_e - \sum_{e,\xi_e} t_{e,\xi_e} e^{i\gamma_e} \bar{\Psi}_{e+\xi_e} \Psi_e \qquad (3)$$

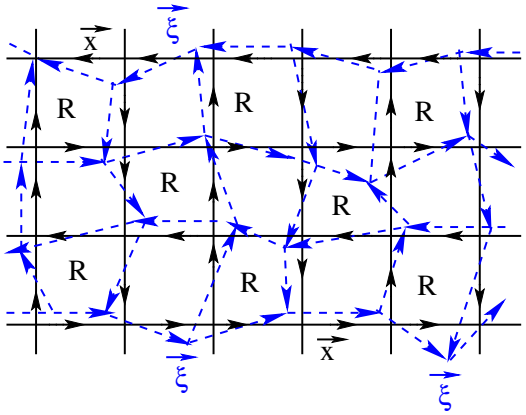

Figure 3. Weakly random medial lattice.

represents hopping of fermions and bosons on the random medial lattice, and the hopping amplitudes take values r and $\pm t$ depending on the vector ξ_e.

The supersymmetry method of Refs. [71, 72 is only suitable for single-particle problems, while the approach of Refs. [74–78] is able, in principle, to describe interacting particles. To this end one uses the second quantization, and the scattering matrices at the nodes are "promoted" to R-matrices acting in the Fock spaces attached to edges of the network (see Fig. 2, right). On a random medial lattice the R-matrices are represented by the quadrangular faces surrounding the scattering nodes, see Fig. 1. The trace of the product of the R-matrices over all nodes of the network gives the partition function. For non-interacting electrons one can use supersymmetry to evaluate the partition function in the basis of (super)coherent states for each of the (super)Fock spaces on the edges. This again gives the action (3).

III. CONTINUUM LIMITS

For the regular CC model the medial lattice is the square lattice with vertices labeled by the Cartesian coordinates x^μ ($\mu = 1, 2$). The vectors ξ_e are $\pm\epsilon\hat{x}_\mu$, where $\hat{x}_\mu$ are unit vectors, and ϵ is the lattice spacing. Near the critical point of the CC model ($t_c = r_c = 1/\sqrt{2}$) the variations of the phases γ_e and the fields Ψ_e are slow, and we can pass to a continuum limit by expanding $\Psi_{x+\epsilon\hat{x}_\mu} \approx (1+\epsilon\partial_\mu)\Psi_x$ and rescaling the fields $\Psi(x)$ in the continuum. In the limit we obtain, as in Ref. [40], the action of the Dirac fermions (and their bosonic partners)

$$S = \int d^2x\, \bar{\Psi}\big[\sigma^\mu\big(i\overleftrightarrow{\partial}_\mu + A_\mu\big) + m\sigma^3 + V\big]\Psi, \qquad (4)$$

where $\overleftrightarrow{\partial}_\mu = (\vec{\partial}_\mu - \overleftarrow{\partial}_\mu)/2$, the mass $m \propto r - r_c$, and the (random) gauge $A_\mu(x)$ and scalar $V(x)$ potentials arise as certain combinations of the random phases $e^{i\gamma_e}$.

Let us now consider the random medial lattice shown in Fig. 3 that is close to the square lattice. Its faces are still quadrangles, and we can introduce (curvilinear) coordinates ξ^a ($a = 1, 2$) following the vectors ξ_e in a natural way. It is clear that the physics cannot depend on the choice of coordinates, so we can use either ξ^a or x^μ coordinates. We can use the formalism of frames of differential geometry[79] to relate coordinate and orthonormal bases of vectors $\hat{x}_\mu = e^a_\mu \partial/\partial\xi^a$ and forms $dx^\mu = e^\mu_a d\xi^a$, as well as the volume elements $d^2x = e\, d^2\xi$, where $e = \det e^\mu_a$. The action (4) written in arbitrary coordinates and invariant under coordinate changes becomes

$$S = \int d^2\xi\, e\, \bar{\Psi}\big[\sigma^\mu e^a_\mu\big(i\overleftrightarrow{\partial}_a + A_a\big) + m\sigma^3 + V\big]\Psi. \qquad (5)$$

The action (5) is that of 2D fermions interacting with random gauge and scalar potentials as well as random geometry (gravity). In the case of weakly deformed lattices, Eqs. (4) and (5) are equivalent, they both describe the system on a flat surface. We propose that random frames can account for more complicated situations that correspond to curved surfaces represented by random graphs.

For discrete random networks a nonzero curvature is associated with the presence of polygons with the number of sides $n \neq 4$. Indeed, imagine the random quadrangulation of the plane dual to a given random network, see the left panel in Fig. 7. An n-gon of the random network corresponds to n quadrangles meeting at a vertex of the dual quadrangulation. One needs to think of all quadrangles as equal squares with $\pi/2$ angles at all four corners. Then it is clear that connecting n such squares at a vertex creates a deficit angle $(4-n)\pi/2$ and distorts the surface into a cone (with positive curvature) if $n < 4$ or a saddle point (with negative curvature) if $n > 4$.

In the continuum, on a curved surface, we define frames and coordinates locally on a given coordinate chart. When charts overlap, there are different coordinate systems on the overlaps, and different expressions for the action. However these expressions are equal due to their invariance under any coordinate transformation $\tilde{\xi}^a = f_a(\xi^1, \xi^2)$. (For discrete random networks we show such overlapping charts in Fig. 6.) In the end the action is still given by Eq. (5), but now we are supposed to consider "arbitrary" frame configurations and average over them. These arguments leave open the question of the functional measure on random surfaces. We believe that the requirements of diffeomorphism and conformal invariance determine the measure uniquely, the same way it is fixed in string theory.[80]

The need to average observables over random geometry means that our system is coupled to *quenched* quantum gravity, see Ref. [81] and references therein. However, in the supersymmetry formalism the partition function of a disordered system is always unity (implying $c = 0$ for the CFT of the critical point), and there is no difference between quenched and annealed gravity.

It is known that 2D quantum gravity modifies critical exponents of a CFT placed on a fluctuating surface. The modification is related to the fact that models coupled to gravity have larger (coordinate reparametrization) symmetry than the ones on the plane, and is given

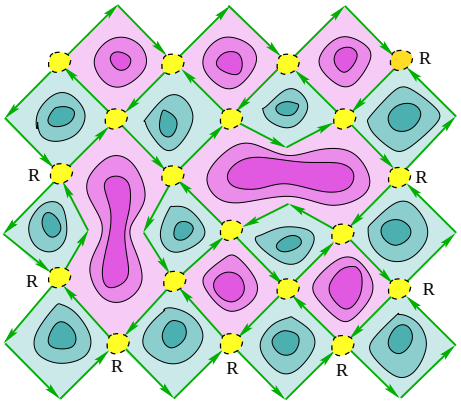

Figure 4. Modified CC network with two "open" nodes, one in the vertical and one in the horizontal direction.

by the KPZ relation.[59–61] The relation has been verified by solutions of critical models of statistical mechanics (related to the so-called minimal CFTs[82]) defined on random graphs.[62–65] When $c = 0$, as for Anderson transitions and critical percolation, the relation is

$$\Delta = \frac{1}{2}(\sqrt{1 + 12\Delta_0} - 1), \tag{6}$$

where Δ_0 (Δ) are scaling dimensions of operators on a flat (fluctuating) surface. Whether this relation can explain the difference between ν and $\nu_{\rm exp}$ is to be seen. However, Eq. (6) should be applicable to multifractal exponents of critical wave functions at the integer QH transition, as well as other 2D Anderson transitions.

IV. CONSTRUCTION AND SIMULATION OF RANDOM NETWORKS

To simulate random networks numerically, we adopt the following construction. Starting with the regular CC network, at each node we set $t = 0$ with probability p_0, $t = 1$ with probability p_1, and leave the node unchanged with probability $p_c = 1 - p_0 - p_1$. The modified nodes with $t = 0$ ($t = 1$) are "open" in the horizontal (vertical) direction, and opening a node changes the four adjacent square faces into two triangles and one hexagon as seen in Fig. 4. The opening procedure can also be depicted on the medial lattice, see Figs. 5. The distorted medial lattice corresponding to the random network of Fig. 4 is shown in Fig. 6. In this figure we also show two contours whose interiors are coordinate charts that contain portions of regular (or weakly distorted) medial lattices. These charts overlap, and on the overlap one can relate the coordinates defined on the two charts by a coordinate transformation, as we mentioned above.

Repeated opening of nodes can produce tilings of the plane by polygons with arbitrary numbers of sides. At the same time, our construction still allows us to use the transfer matrix of the CC model, but with modified t and r amplitudes.

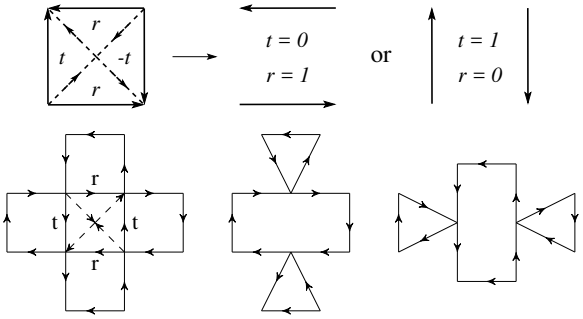

Figure 5. Top: opening a node. Bottom: The resulting modifications of the medial lattice.

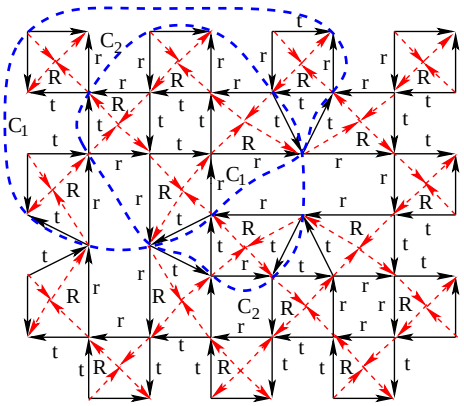

Figure 6. The modified medial lattice corresponding to the network shown in Fig. 4.

To maintain statistical isotropy of the model, we choose $p_0 = p_1$. Then we expect that the critical point is still given by the value $t_c^2 = 1/2$ for the unchanged nodes. Moreover, in this paper we fix

$$p_0 = p_1 = p_c = \frac{1}{3}. \tag{7}$$

To extract the exponent ν for random networks, we use a modification of the transfer matrix method[41,42] developed in Ref. [45]. In the standard transfer matrix method one multiplies many transfer matrixs for a single realization of disorder and relies on the self-averaging property of Lyapunov exponents. This property in the limit of infinite length of the sample is the subject of the central-limit-type theorem for products of random matrices due to Oseledec.[83] The modification of Ref. [45] that we use here, on the other hand, is based on another central-limit-type theorem for products of random matrices due to Tutubalin.[84] This theorem states that the Lyapunov exponents of products of a finite number of random matrices are random numbers whose distribution approaches Gaussian for large sample lengths.

Thus, we simulate ensembles of $N_r = 624$ samples of random networks on strips of widths M (the number of nodes per column) varying from 20 to 200, and of length $L = 5 \cdot 10^6$, and a range of the parameter x which en-

codes deviations of t from t_c. This makes our simulation each pair M, x to be equivalent to the standard transfer matrix simulation of a single sample of effective length $L_{\rm eff} = N_r \times L > 3 \cdot 10^9$, exceeding the longest previously reported sample lengths. For each ensemble of random network we check that the histogram of the smallest Lyapunov exponents is close to a Gaussian, see details in Appendices.

We use the so-called LU decomposition of transfer matrices.[48] Since t and r appear in the denominators of the matrix elements of transfer matrices, making them zero is a singular procedure, related to the disappearance of two horizontal channels upon opening a node in the vertical direction. To overcome this difficulty, for every open node we take either t or r to be equal to $\varepsilon \ll 1$. We then look at how the resulting Lyapunov exponents depend on ϵ. We found that the results saturate at $\varepsilon = 10^{-5}$, and there are no changes when reducing ϵ to 10^{-7}. For even smaller ε the results start changing again. This is to be expected because the large differences of values in the entries of transfer matrices cause numerical instabilities for the LU decomposition. We have chosen $\varepsilon = 10^{-6}$ for our calculations.

The smallest Lyapunov exponent γ is expected to have the following finite-size scaling behavior:

$$\gamma M = \Gamma[M^{1/\nu} u_0(x), M^y u_1(x)]. \tag{8}$$

Here $u_0(x)$ is the relevant field and $u_1(x)$ the leading irrelevant field. The relevant field vanishes at the critical point, and $y < 0$. At the fixed point of the infinite system Γ takes a universal value Γ_c that is related to the multifractal exponent α_0 by[44]

$$\Gamma_c = \pi(\alpha_0 - 2). \tag{9}$$

The fitting and the error analysis of our numerical data are presented in Appendices. The results of the analysis are

$$\nu = 2.372 \pm 0.017, \qquad y = -0.61 \pm 0.07, \tag{10}$$

$$\Gamma_c = 0.866 \pm 0.004, \qquad \alpha_0 - 2 = 0.276 \pm 0.001, \tag{11}$$

where the errors are given by confidence bounds with 95% significance level. The closeness of our value for ν to $\nu_{\rm exp}$ is likely a coincidence, since we did not take into account the Coulomb interaction. However, our values for ν and Γ_c (and $\alpha_0 - 2$) are significantly different from these quantities for the CC model where $\alpha_0 - 2 \approx 0.25$.[43,46,85,86] The difference shows that structural disorder is, indeed, a relevant perturbation that modifies the critical behavior of the network model.

V. OTHER SYMMETRY CLASSES

Network models can be constructed for all 10 symmetry classes of disordered systems identified in Refs. [66, 67. Superconductors with broken time-reversal invariance in 2D can exhibit QH transitions where the spin

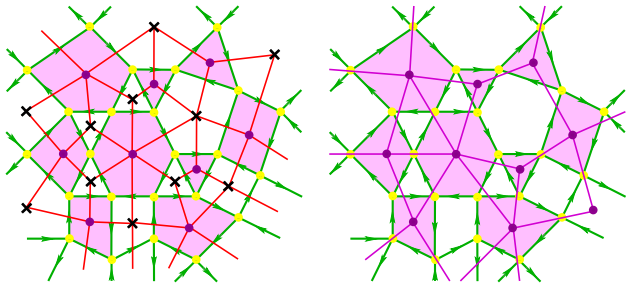

Figure 7. Left: original random network and its dual. Right: percolation lattice.

(class C)[87,88] and thermal (class D)[89] Hall conductivities jump in quantized units. The ideas developed above apply to network models for these transitions. In addition, both spin QH transition and thermal QH transition are simpler than the integer QH transition since many of their properties can be determined from mappings to classical models.

The regular network in class C maps to classical bond percolation on a square lattice,[90–92] for which many exact results are known. The mapping has lead to a host of exact critical properties at the spin QH transition[90,92–97] and was extended to arbitrary graphs.[72]

The graphs relevant for our study are shown in Fig. 7. For a given random network we draw the dual bipartite graph with dots on the shaded faces and crosses on the empty faces of the original random network. The dual graph forms a random quadrangulation of the plane. Dissecting all quadrangles by diagonals connecting the dots and removing the crosses and all edges connected to them, results in a lattice (Fig. 7) on which the bond percolation should be considered.

Critical bond percolation on random quadrangulations (or their duals) was considered in Ref. [64], and it was shown that the KPZ relation (6) is valid in this case. We believe that the spin QH transition on random networks lies in the same universality class, and that Eq. (6) can be applied to all critical exponents obtained in Refs. [90, 92, 94–97]. This includes, in particular, the dimension of the "two-leg" operator that determines the localization length exponent ν, as well as a few multifractal exponents.

The thermal QH transition in class D can also be described and simulated by a network model.[98–101] Its effective field theory (without geometric disorder) is given by the Majorana fermions with random mass, the same theory that describes the critical Ising model with a weak bond disorder.[89,102] The random mass is a marginally irrelevant perturbation, and critical exponents at the transition are given by their Ising model values. When the model is coupled to 2D quantum gravity, we still should consider the quenched situation, and the critical exponents should be modified according to Eq. (6.

VI. DISCUSSION AND OUTLOOK

The geometric disorder that we simulate by a modified CC model can be viewed as randomness in the heights V of the saddle points in the disorder potential. Indeed, it is known that (at zero energy) $t^2 = (1 + e^{-V})^{-1}$.[103] Our choice of t is described by the tri-modal distribution

$$P(V) = p_0\delta(V - 2\ln\varepsilon) + p_c\delta(V) + p_0\delta(V + 2\ln\varepsilon). \tag{12}$$

Previous studies of random V[70,104,105] focused on the uniform distribution in $V \in [-W, W]$ or the bimodal distribution

$$P(V) = \frac{1}{2}[\delta(V - W) + \delta(V + W)]. \tag{13}$$

No choice of W gives our type of randomness when $p_c > 0$. However, for $p_c = 0$ our distribution becomes bimodal, and describes classical critical percolation with $\nu = 4/3$. The other extreme, $p_c = 1$, gives the regular CC model.

We stress here that the regular CC model essentially differs from random network because for any $p_c < 1$ there is geometric disorder: the fluctuating metric of the 2D quantum gravity. This is a new dynamical field, and the theory in the continuum is invariant under coordinate reparametrizations. This symmetry is absent in the continuum limit of the regular CC model. Thus we expect models with $p_c < 1$ to be in a new universality class, different from that of the CC model. At present we have sufficient data only for $p_c = 1/3$, so we can envision two possible scenarios: 1) a novel fixed point at a finite p_c, 2) a line of fixed points between $p_c = 0$ and $p_c = 1$. Both scenarios are very interesting and have not appeared in the integer QH transition literature before. Simulations for other values of p_c are in progress, and will allow us to determine which scenario is actually realized.

We plan to simulate random networks in classes C and D, and solve the classical percolation problem on relevant graphs using matrix models techniques. We will, furthermore, consider the problem of Dirac fermions in an Abelian random gauge potential coupled to 2D quantum gravity, and determine the multifractal spectrum of the wave functions in order to test the applicability of the KPZ relation (6).

In summary, we have considered the possibility that a certain type of geometric disorder, previously missed in the study of the integer QH transition, changes its universality class. Our numerical simulations support this idea. We propose that the proper framework for a field-theoretic description of this type of disorder is provided by 2D quantum gravity coupled to matter fields. These ideas can be applied to other 2D Anderson transitions.

ACKNOWLEDGMENTS

A. S. thanks the Theoretical Physics group at Wuppertal University for hospitality. A. S. and A. K. acknowledge support by DFG grant KL 645/7-1. A. S. was partially supported by ARC grant 15T-1C058. I. G. was partially supported by the NSF Grant No. DMR-1508255. We are grateful to R. A. Roemer and A. W. W. Ludwig for helpful discussions. Extensive calculations have been performed on Rzcluster (Aachen), PC^2 Paderborn) and particularly on JUROPA (Jülich). The authors gratefully acknowledge the computing time granted by the John von Neumann Institute for Computing (NIC) and provided on the supercomputer JUROPA at Jülich Supercomputing Centre (JSC).

Appendix A: Model description

For the calculation of critical indices we used a variant of the transfer-matrix method developed in Refs. [41, 42]. To calculate the smallest Lyapunov exponent of the CC-model it is necessary to calculate a product

$$T_L = \prod_{j=1}^{L} M_1 U_{1j} M_2 U_{2j} \tag{A1}$$

of layers of transfer matrices $M_1 U_{1j} M_2 U_{2j}$ corresponding to two columns M_1 and M_2 of vertical sequences of 2x2 scattering nodes,

$$M_1 = \begin{pmatrix} B^1 & 0 & \cdots & 0 \\ 0 & B^1 & \ddots & \vdots \\ \vdots & \ddots & \ddots & 0 \\ 0 & \cdots & 0 & B^1 \end{pmatrix} \tag{A2}$$

and

$$M_2 = \begin{pmatrix} B^2_{22} & 0 & \cdots & 0 & B^2_{21} \\ 0 & B^2 & \ddots & & 0 \\ \vdots & \ddots & \ddots & & \vdots \\ 0 & & & B^2 & 0 \\ B^2_{12} & 0 & \cdots & 0 & B^2_{11} \end{pmatrix} \tag{A3}$$

with

$$B^1 = \begin{pmatrix} 1/t & r/t \\ r/t & 1/t \end{pmatrix} \qquad \text{and} \qquad B^2 = \begin{pmatrix} 1/r & t/r \\ t/r & 1/r \end{pmatrix} \tag{A4}$$

This choice of the transfer matrices corresponds to the periodic boundary condition in the transverse direction. In other words, these transfer matrices describe the CC network model on a cylinder.

The U-matrices have a simple diagonal form with independent phase factors $U_{nm} = \exp(i\alpha_n)\,\delta_{nm}$ for $U = U_{1j}$ and U_{2j}. Here t and r are the transmission and reflection amplitudes at each node of the regular lattice which are parameterized by

$$t = \frac{1}{\sqrt{1 + e^{2x}}} \qquad \text{and} \qquad r = \frac{1}{\sqrt{1 + e^{-2x}}}. \tag{A5}$$

The parameter x corresponds to the Fermi energy measured from the Landau band center scaled by the Landau band width (with the critical point at $x = 0$). The phases α_n are random variables uniformly distributed in the range $[0, 2\pi)$, reflecting that the phase of an electron approaching a saddle point of the random potential is arbitrary.

To simulate random networks numerically, we remove scattering nodes by opening them in horizontal or vertical direction with probabilities p_0 and p_1 by adopting the following construction. Starting with the regular CC network, at each node we set $t = \varepsilon \ll 1$ with probability p_0, $t = \sqrt{1-\varepsilon^2}$ with probability p_1, or leave the node unchanged with probability $p_c = 1 - p_0 - p_1$. Here the small number ε is chosen as $\varepsilon = 10^{-6}$: We found that the results saturate already at $\varepsilon = 10^{-5}$, and there are no changes when reducing ε to 10^{-7}. For even smaller ε the results start changing again due to precision issues of the numerics.

In table I we present results for Lyapunov exponents of a series of ensembles for same x and M ($x = 0.01$, $M = 50$, $L = 1\,000\,000$ and ensemble size 10) and different values for ϵ. The numbers show that from the third to the second last column there is a stable regime where the ensemble mean agrees within the error bars. For larger ϵ the approximation is not so good and for smaller ϵ the matrix product is ill conditioned. We found that $\epsilon = 10^{-6}$ is the smallest choice within the stable regime. Therefore this value has been our choice for ϵ for further calculations.

Furthermore, we found that the results for the Lyapunov exponents for longer chains depend less on the value of ϵ than for shorter chains. We found this by generating a series of random numbers which we then used for the computation of the Lyapunov exponent of chains of length $L = 10^6$ to 10^7 for four different values of ϵ (and $M = 70$ and $x = 0.08$). For each value of L, but different values of ϵ we used the same series of random numbers. The results show a convincing convergence: for $L = 10^6$ the relative error is 1/100, whereas it is 1/1000 for $L = 10^7$. We are convinced that this trend continues for even larger values of L, but for programming reasons (parallelization and other technical issues) we had to work with large ensembles of reasonably long chains. Furthermore, in this paper we use $p_0 = p_1 = p_c = 1/3$.

Appendix B: The fitting procedure

As is standard in the transfer matrix method, we want to numerically estimate the Lyapunov exponent γ defined as the smallest positive eigenvalue of

$$\frac{1}{2L}\log[T_L T_L^\dagger]. \tag{B1}$$

in the limit as $L \to \infty$. This quantity is self-averaging, and for finite L it's distribution is basically Gaussian. We numerically calculate γ for various combinations of the parameter x and the lattice width M. The results are shown in Fig. 8.

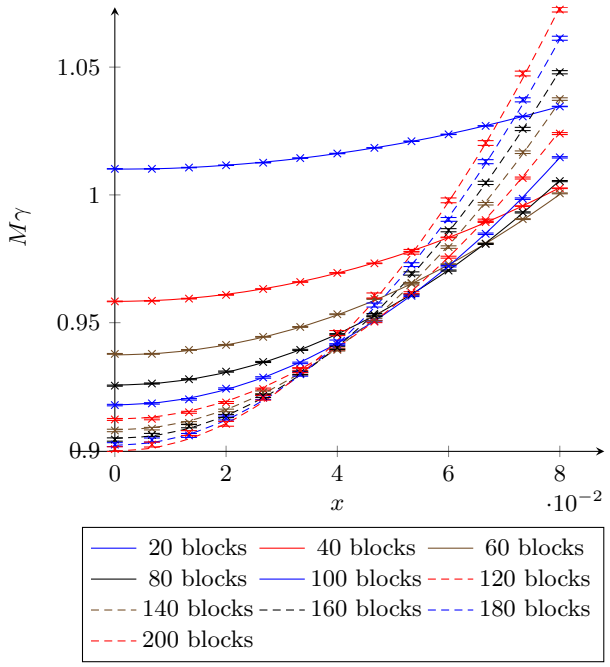

Figure 8. Plot of the logarithm of the smallest eigenvalue of the transfer matrix times M (= number of blocks) depending on the distance x from the critical point. The x-values divide the interval $[0, 0.08]$ into 12 equal parts. The data points are given by the average of the ensemble belonging to the corresponding values for x and M. All considered values for M are listed in the legend. The product length is $L = 5\,000\,000$. The error bars are obtained from the standard deviation of this ensemble. The curves are obtained by plotting the fit function for the relevant values of M in the regime $x = 0$ to $x = 0.08$. Each ensemble consists of 624 eigenvalues.

It is clearly seen that the lines corresponding to different values of M do not intersect at the critical value $x = 0$. In fact, they do not intersect at a single point at all. Therefore, any attempt at trying to use a single-parameter scaling to collapse the data is doomed to fail. The reason for this is that the critical point of the CC model is not the same as the fixed point. They differ by the presence of irrelevant variables that decay as we increase the system width. For the CC model specifically, the leading irrelevant variable has the scaling exponent $y < 0$ which is rather small in magnitude. This causes strong correction to scaling even at the critical point. This is a known feature of the CC model that has been stressed by Slevin and Ohtsuki in Ref. [43]. They emphasized that it is crucial to include irrelevant scaling variables as arguments of the fitting functions used in the scaling analysis of the data. This procedure leads to much more reliable results, but cannot be visualized as a simple scaling collapse of the numerical data, as in the case of a single-variable scaling. Inclusion of irrelevant variables in the scaling analysis has become a standard procedure in the numerical studies of network models,

ϵ	$9.12 \cdot 10^{-4}$	$3.35 \cdot 10^{-4}$	$1.23 \cdot 10^{-4}$	$4.54 \cdot 10^{-5}$	$1.67 \cdot 10^{-5}$	$6.14 \cdot 10^{-5}$	$2.26 \cdot 10^{-6}$	$8.32 \cdot 10^{-7}$
$\bar{\gamma}$	0.9448	0.9515	0.9529	0.9534	0.9531	0.9542	0.9547	0.9508
σ	0.0017	0.0019	0.0019	0.0021	0.0022	0.0021	0.0021	0.0022

Table I. For an ensemble with the same values for x and M but different ϵ the ensemble mean and the standard deviation have been calculated. The numbers show that there is a stable regime where the differences of the ensemble mean are less than the standard deviation. This data set is caracterized by the following parameters: $x = 0.01$, $M = 50$, $L = 1\,000\,000$ and an ensemble size of 10 Lyapunov exponents.

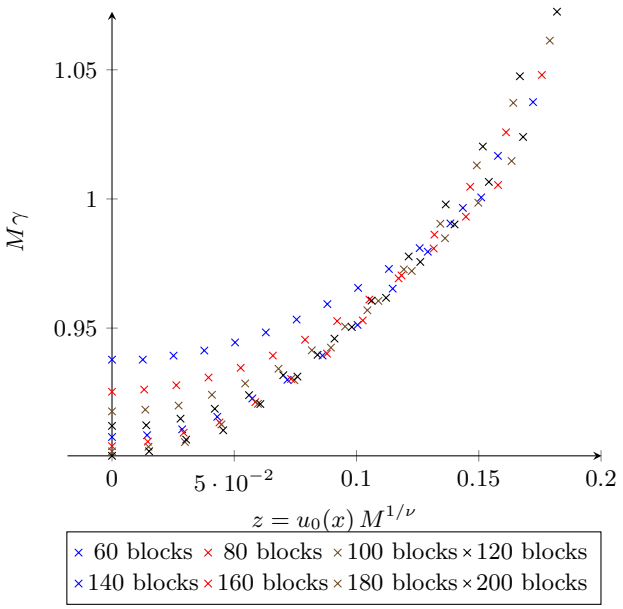

Figure 9. One parameter fit, M=20, 40 excluded.
Fit in numbers:
$g(x, M) = G_0 + G_2\,(xM^{1/\nu})^2$
Coefficients (with 95% confidence bounds):
$G_0 = 0.9266$ (0.9242, 0.929)
$G_2 = 3.343$ (1.572, 5.114)
$\nu = 6.446$ (4.024, 8.869)

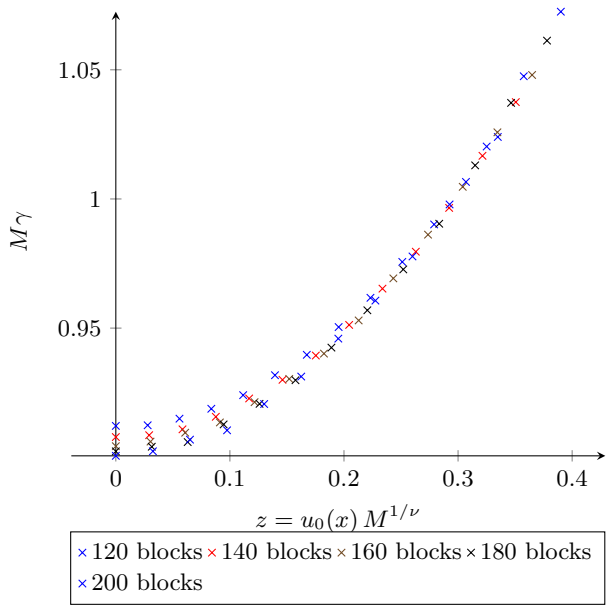

Figure 10. One parameter fit, M=20, ... , 100 excluded.
Fit in numbers:
$g(x, M) = G_0 + G_2\,(xM^{1/\nu})^2$
Coefficients (with 95% confidence bounds):
$G_0 = 0.908$ (0.907, 0.909)
$G_2 = 1.052$ (0.7277, 1.376)
$\nu = 3.344$ (3, 3.688)

and here we follow the same procedure.

Thus, we will fit the scaling behavior of the Lyapunov exponent γ near the critical point to the following expression:

$$\gamma \cdot M = \Gamma(M^{1/\nu} u_0, M^y\, u_1), \tag{B2}$$

Here we have taken into account the relevant field with exponent ν and the leading irrelevant field with exponent y. M is the number of 2×2 blocks in the transfer matrices (= half the number of horizontal channels of the lattice), $u_0 = u_0(x)$ is the relevant field and $u_1 = u_1(x)$ the leading irrelevant field. It is known that the relevant field vanishes at the critical point, and that $y < 0$.

Before proceeding with the two-variable fits, let us illustrate the point made above about the inadequacy of the single-variable fit. Figs. 9 and 10 show attempts at scaling collapse using the fitting function where only the relevant scaling field is retained: $\gamma \cdot M = \Gamma(M^{1/\nu} u_0)$. We see that both attempts produce rather poor scaling collapse even after we discard the data with $M = 20, 40$ (Fig. 9) or data with $M = 20, \ldots, 100$ (Fig. 10). The value of the fit parameters shown in the figure captions cannot be trusted, and, in particular, the two values of the ν exponents obtained in this single-variable fits are extremely unreliable.

Coming back to the two-variable fit, on the left hand side of Eq. (B2) we use the numerical results for the eigenvalues of T_L, where we are particularly interested in the eigenvalue closest to 1. The right hand side of (B2) is expanded in a series in x and powers of M, and the expansion coefficients are obtained from a fit. Some coefficients in this expansion vanish due to a symmetry argument.[43] If x is replaced by $-x$ we see from (A5) that t turns into r and vice versa. Due to the periodic boundary conditions the lattice is unchanged. Therefore the left hand side of (B2) is invariant under the sign change of x. Hence the right hand side must be even in x. That renders $u_0(x)$ and $u_1(x)$ either even or odd

in x. For the Chalker Coddington network the critical point is at $x = 0$. This lets us choose $u_0(x)$ odd and $u_1(x)$ even. The fit now should use as few coefficients as possible while reproducing the data as closely as possible.

The scaling function Γ in the right side of (B2) is expanded in the fields u_0 and u_1 yielding

$$\begin{aligned}\Gamma(u_0(x)M^{1/\nu}, u_1(x)M^y) &= \Gamma_c + \Gamma_{01}u_1M^y + \Gamma_{20}u_0^2M^{2/\nu} \\ &+ \Gamma_{02}u_1^2M^{2y} + \Gamma_{21}u_0^2u_1M^{2/\nu}M^y + \Gamma_{03}u_1^3M^{3y} \\ &+ \Gamma_{40}u_0^4M^{4/\nu} + \Gamma_{22}u_0^2M^{2/\nu}u_1^2M^{2y} + \Gamma_{04}u_1^4M^{4y} + \dots\end{aligned} \tag{B3}$$

We further expand u_0 and u_1 in powers of x as was done, for example, in Refs. [43, 45]:

$$u_0(x) = x + \sum_{k=1}^{\infty} a_{2k+1}x^{2k+1} \quad \text{and} \quad u_1(x) = 1 + \sum_{k=1}^{\infty} b_{2k}x^{2k}. \tag{B4}$$

In Eq. (B3) we retained only terms that are even in x. Because of the ambiguity in the overall scaling of the fields, the leading coefficient in Eq. (B4) can be chosen to be 1.

The first term in the expansion (B3), Γ_c represents the asymptotic value of the universal critical amplitude ratio Γ in the infinite system. Theoretical arguments based on conformal invariance relate Γ to the multifractal exponent α_0:

$$\Gamma_c = \pi(\alpha_0 - 2), \tag{B5}$$

see, for example, Ref. [44].

1. Weights and Errors

The left hand side of Eq. (B2) is determined by the results of numerical simulations of the random network model. Following Ref. [45] we have produced large ensembles of the Lyapunov exponent γ by simulating many disorder realizations for many combinations of x and M. We calculated 624 disorder realizations for any combination of $M = 20, 40, 60, 80, 100, 120, 140, 160, 180, 200$ and $x = 0.08/12 \cdot [0, 1, 2, 3, 4, 5, 6, 7, 8, 9, 10, 11, 12]$ for fixed $L = 5\,000\,000$. Our goal is to check whether the central limit theorem[84] also works in the case of randomness of the network or not. Fig. 11 shows the distribution of the Lyapunov exponent for $M = 60$ and $x = 0.02$ being nicely described by a Gaussian which demonstrates the validity of the central limit theorem.

In the fitting procedure, the weight of each such γ is given by the reciprocal of the variance of the corresponding ensemble. So all γ from the same (x, M) ensemble enter the fit with the same weight. On the right hand side of Eq. (B2) the fitting formula depending on x and M is used. The coefficients of the expansion and the critical exponents are the fitting coefficients.

The fits are performed in several steps. First a weighted nonlinear least square fit based on a trust region algorithm with specified regions for each parameter is applied. The resulting parameters are used in a further weighted nonlinear least square fit based on a trust region algorithm. Here no limits are imposed on the fit parameters. The last step is repeated until the resulting parameters stop changing.

2. Evaluation of fits

The next step is the evaluation of the fit results. We present several methods to do this.

Very common is the χ^2-*test*. χ^2 is given by

$$\chi^2 = \sum_i \frac{(y_i - f_i)^2}{\sigma_i^2} \tag{B6}$$

where f_i is the value predicted by the fit and y_i the measured value. The σ_i are given by the standard deviation of the ensemble with the corresponding values for x and M. As our fit contains large ensembles of data points for the same (x, M) coordinates, $\chi^2 = 0$ is not possible, actually it will be large due to the huge number of data points. The way to deal with this behavior is to consider the ratio $\chi^2/$*degrees of freedom*. The expectation value for this ratio is 1 for an ideal fit. The *degrees of freedom* is the number of data points in the fit minus the number of fit parameters.

Deviations from 1 are evaluated by use of the cumulative probability $P(\tilde{\chi}^2 < \chi^2)$ which is the probability of observing – just for statistical reasons – a sample statistic with a smaller χ^2 value than in our fit. A small value of P, i.e. a large value of the complement $Q := 1 - P$ is taken as indicative for a good fit. However, values of P lower than $1/2$ indicate problems in the estimation of the error bars of the individual data points.

Another criterion is based on the width of the *confidence intervals*. This quantifies the quality of the prediction for a single parameter. We use 95% confidence intervals which means that for repeated independent generation of the same amount of data and application of the same kind of data analysis the resulting confidence intervals contain the true parameter values in 95% of the cases.

A most sensitive criterion is the *Akaike information criterion* (AIC).[106] AIC is founded on information theory; Akaike found a formal relationship between Kullback-Leibler information and likelihood theory. This finding makes it possible to combine estimation (i.e., maximum likelihood or least squares) and model selection under a unified optimization framework.

Unlike in the case of hypothesis testing, AIC does not assume that the correct model is among the tested models. AIC rather offers a relative estimate of the information lost when a given model is used to represent the process that generates the data. This way, given a collection of models, AIC ranks those models if they are based on the same data. In this case a comparison to the best model can be calculated easily. In case a different

data base has been used, the models cannot be ranked or compared.

For the calculations presented in this article we have been using the AICc, which is a small sample version of AIC or, more precisely, a second order bias correction. AICc is also valid if k is not small compared to n, where n denotes the sample size and k denotes the number of parameters, and is given by

$$\mathrm{AICc} = \mathrm{AIC} + \frac{2k(k+1)}{n-k-1}. \tag{B7}$$

This formula holds exactly if the model is univariate, linear, and has normally-distributed residuals, but may in other cases still be used unless a more precise correction is known. Further details on the AIC and the AICc can be found in Ref. [107].

The AIC can be expressed in terms of χ^2:

$$\mathrm{AIC} = 2k + \chi^2 - 2C \tag{B8}$$

Here $2C$ is a constant (dependent on the set of data points) that can be omitted because for comparisons we only need differences of AICc's.

For comparing models, the AIC (and the AICc) are used in the following way. Suppose, we have l models with $\mathrm{AIC}_1, \ldots \mathrm{AIC}_l$. The model with the smallest AICc — let us call it AIC_{min}, — is the favorite one. The relative probability of model j compared to the model with AIC_{min} is

$$\exp \frac{\mathrm{AIC}_{min} - \mathrm{AIC}_j}{2}. \tag{B9}$$

Note that the exponential expression is smaller than one.

The last criterion we present is the sum of *residuals*. It is given by $res = \sum_j res_j$, $res_j = y_j - f_j$. The sum of residuals should be small compared to the number of degrees of freedom. The residuals plotted should look like noise around zero. If the residuals significantly deviate from zero, we expect that the fit function is not correct.

Appendix C: Results

In Fig. 11 we present an example of the distribution of Lyapunov exponents for fixed width M, parameter x and chain length L. This distribution defines the data point and its accuracy for the combination (x, M). The reciprocal of the variance is used as the weight the data point carries in the fitting procedure.

In Fig. 8 we present the product $M\gamma$ (the left-hand side of Eq. (B2)) versus x for various values of the width M. The corresponding fitting parameters are presented in the table below. The lines through the data are the plots of the right-hand side of Eq. (B3). The agreement we get here with a two-variable fit is excellent, as is seen from the figure.

Our best fitting results have been obtained by expanding Γ up to second order in u_0 and u_1 (B3), and expanding u_0 (u_1) up to the third (second) order in x. We found the following coefficients and goodness of fit parameters:

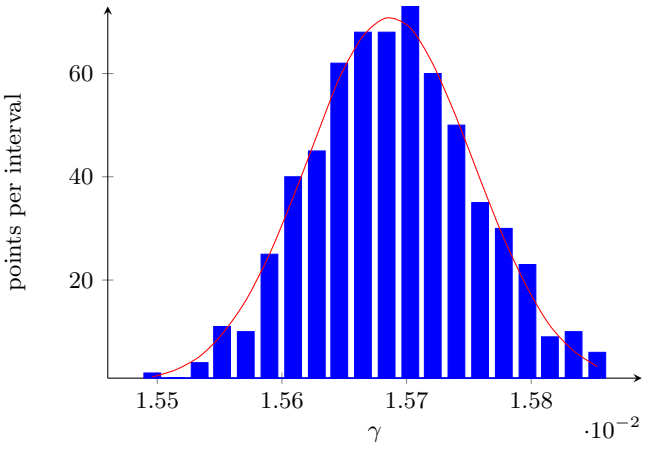

Figure 11. Distribution of Lyapunov exponents in the ensemble of calculations with 624 elements for chain length $L = 5\,000\,000$, $M = 60$ and $x = 0.02$.

Coefficients (confidence bounds 95%):

$\Gamma_c =$	0.866	$(0.862, 0.870)$
$\Gamma_{01} =$	0.842	$(0.612, 1.071)$
$\Gamma_{02} =$	0.352	$(-0.043, 0.747)$
$\Gamma_{20} =$	0.311	$(0.302, 0.320)$
$a_3 =$	0.287	$(-0.227, 0.801)$
$b_2 =$	-0.411	$(-0.793, -0.029)$
$\nu =$	2.372	$(2.355, 2.389)$
$y =$	-0.611	$(-0.678, -0.545)$

Goodness of fit parameters:

χ^2:	81190.6
degrees of freedom (dof) :	81112
χ^2/dof:	1.001
P:	0.578
AICc:	-556358.5
sum of residuals:	203.57

The degrees of freedom have been calculated from the number of data points $624 \cdot 13 \cdot 10$ minus 8, the number of fit parameters. We see χ^2/dof is close to 1 and the cumulative probability $P = 0.554$ is close to 1/2, marking a good fit result. The sum of residuals is small compared to the number of degrees of freedom. As can be seen in Fig. 12, the residuals are distributed around zero as judged by the eye. All this indicates that the fit is reliable and the data agree with the model equation.

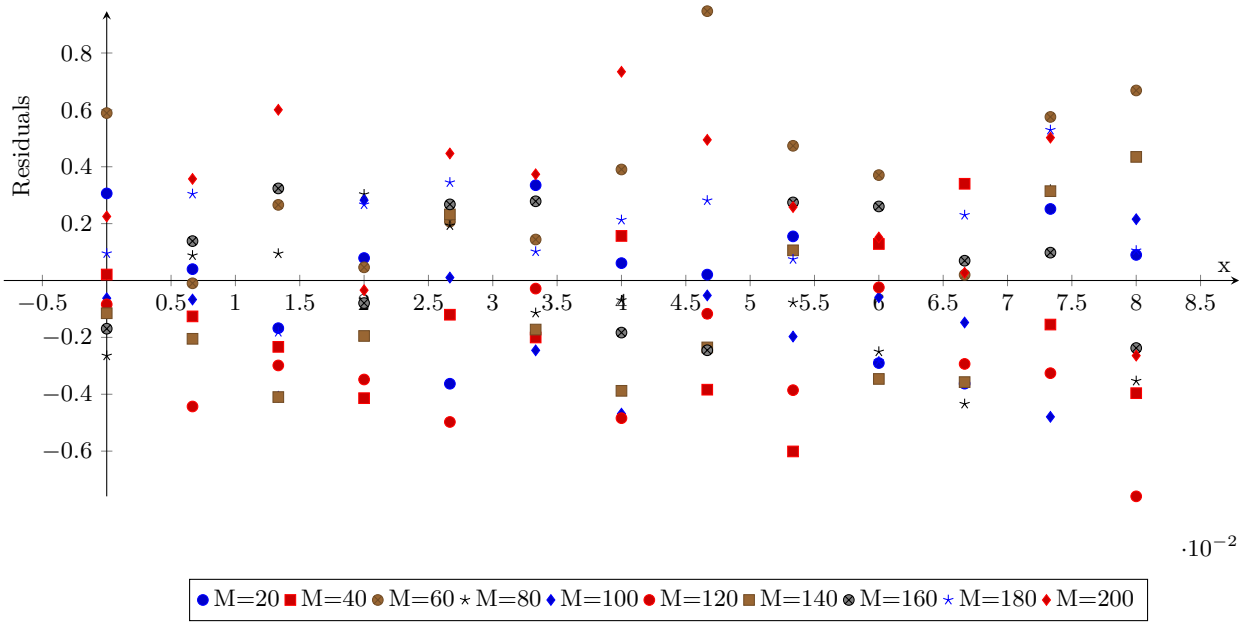

Figure 12. This figure presents a plot of the residuals. The x-axis shows the scaling parameter x and the y-axis the residuals. For each pair (x, M) the corresponding residuals are summed up and the result is shown in the plot. By inspection the x-axis is at the center of the scattered residuals. This indicates that there is no systematic deviation between the data points and the model equation.

An alternative data analysis would use averaging over the 624 randomness realizations for each combination of (M, x) and subjecting the results (mean value and variance) to the fit routine. This routine would then deal with $10 \cdot 13$ data points, but yields the same result as the procedure described above: One can easily show that the χ^2 values of the two procedures differ just by a constant $(10 \cdot 13 \cdot 623)$.

We performed a set of additional fits for different orders of expansions of Γ. In the third order we obtain $\nu = 2.38$ differing only weakly from the second order result $\nu = 2.372$. We also carried out the fit procedure for restricted data sets with M ranging from 20 to some $M_{\max}$ for different values of $M_{\max}$. For $M_{\max} = 100, 140, 180, 200$ we obtain $\nu = 2.405, 2.385, 2.37, 2.372$. From this extremely weak size dependence we exclude the possibility of a crossover scenario from percolation to CC criticality.

Fits with two irrelevant fields are clearly discouraged by the Akaike criterion. Those models produce a (relative) Akaike coefficient of at least AICc $= -556340$. Therefore their relative likelihood is about 0.0003.

[1] B. Huckestein, Rev. Mod. Phys. **67**, 357 (1995).
[2] F. Evers and A. D. Mirlin, Rev. Mod. Phys. **80**, 1355 (2008).
[3] H. P. Wei, D. C. Tsui, M. A. Paalanen, and A. M. M. Pruisken, Phys. Rev. Lett. **61**, 1294 (1988).
[4] S. Koch, R. J. Haug, K. v. Klitzing, and K. Ploog, Phys. Rev. B **43**, 6828 (1991).
[5] S. Koch, R. J. Haug, K. v. Klitzing, and K. Ploog, Phys. Rev. Lett. **67**, 883 (1991).
[6] S. Koch, R. J. Haug, K. v. Klitzing, and K. Ploog, Phys. Rev. B **46**, 1596 (1992).
[7] L. W. Engel, D. Shahar, Ç. Kurdak, and D. C. Tsui, Phys. Rev. Lett. **71**, 2638 (1993).
[8] H. P. Wei, L. W. Engel, and D. C. Tsui, Phys. Rev. B **50**, 14609 (1994).
[9] W. Li, G. A. Csáthy, D. C. Tsui, L. N. Pfeiffer, and K. W. West, Phys. Rev. Lett. **94**, 206807 (2005).
[10] W. Li, C. L. Vicente, J. S. Xia, W. Pan, D. C. Tsui, L. N. Pfeiffer, and K. W. West, Phys. Rev. Lett. **102**, 216801 (2009).
[11] A. M. M. Pruisken and I. S. Burmistrov, ArXiv e-prints (2009), arXiv:0907.0356 [cond-mat.mes-hall].
[12] A. J. M. Giesbers, U. Zeitler, L. A. Ponomarenko, R. Yang, K. S. Novoselov, A. K. Geim, and J. C. Maan, Phys. Rev. B **80**, 241411 (2009).
[13] P. W. Anderson, Phys. Rev. **109**, 1492 (1958).
[14] E. Abrahams, P. W. Anderson, D. C. Licciardello, and T. V. Ramakrishnan, Phys. Rev. Lett. **42**, 673 (1979).
[15] H. Levine, S. B. Libby, and A. M. M. Pruisken, Phys. Rev. Lett. **51**, 1915 (1983).
[16] H. A. Weidenmüller, Nucl. Phys. B **290**, 87 (1987).
[17] D. E. Khmel'nitskiĭ, JETP Lett. **38**, 454 (1983).
[18] A. M. M. Pruisken, Phys. Rev. B **32**, 2636 (1985).
[19] V. Gurarie and A. W. W. Ludwig, arXiv eprint (2004), hep-th/0409105.
[20] M. R. Zirnbauer, arXiv eprint (1999), hep-th/9905054.

[21] M. J. Bhaseen, I. I. Kogan, O. A. Soloviev, N. Taniguchi, and A. M. Tsvelik, Nucl. Phys. B **580**, 688 (2000).
[22] A. M. Tsvelik, arXiv eprint (2001), cond-mat/0112008.
[23] A. M. Tsvelik, Phys. Rev. B **75**, 184201 (2007).
[24] A. W. W. Ludwig, M. P. A. Fisher, R. Shankar, and G. Grinstein, Phys. Rev. B **50**, 7526 (1994).
[25] C. de C. Chamon, C. Mudry, and X.-G. Wen, Phys. Rev. B **53**, 7638 (1996).
[26] C. Mudry, C. Chamon, and X.-G. Wen, Nucl. Phys. B **466**, 383 (1996).
[27] C. D. C. Chamon, C. Mudry, and X.-G. Wen, Phys. Rev. Lett. **77**, 4194 (1996).
[28] I. I. Kogan, C. Mudry, and A. M. Tsvelik, Phys. Rev. Lett. **77**, 707 (1996).
[29] Y. Hatsugai, X.-G. Wen, and M. Kohmoto, Phys. Rev. B **56**, 1061 (1997).
[30] H. E. Castillo, C. de C. Chamon, E. Fradkin, P. M. Goldbart, and C. Mudry, Phys. Rev. B **56**, 10668 (1997).
[31] E. Bettelheim, I. A. Gruzberg, and A. W. W. Ludwig, Phys. Rev. B **86**, 165324 (2012).
[32] I. A. Gruzberg, A. W. W. Ludwig, A. D. Mirlin, and M. R. Zirnbauer, Phys. Rev. Lett. **107**, 086403 (2011).
[33] I. A. Gruzberg, A. D. Mirlin, and M. R. Zirnbauer, Phys. Rev. B **87**, 125144 (2013).
[34] R. Bondesan, D. Wieczorek, and M. R. Zirnbauer, Phys. Rev. Lett. **112**, 186803 (2014).
[35] R. Bondesan, D. Wieczorek, and M. R. Zirnbauer, .
[36] J. T. Chalker and P. D. Coddington, J. Phys. C **21**, 2665 (1988).
[37] B. Kramer, T. Ohtsuki, and S. Kettemann, Phys. Rep. **417**, 211 (2005).
[38] N. Read, (1991), unpublished.
[39] M. R. Zirnbauer, Annalen Phys. **3**, 513 (1994), [Erratum: Annalen Phys. **4**, 89 (1995)].
[40] C.-M. Ho and J. T. Chalker, Phys. Rev. B **54**, 8708 (1996).
[41] A. MacKinnon and B. Kramer, Phys. Rev. Lett. **47**, 1546 (1981).
[42] A. MacKinnon and B. Kramer, Z. Phys. B **53**, 1 (1983).
[43] K. Slevin and T. Ohtsuki, Phys. Rev. B **80**, 041304 (2009).
[44] H. Obuse, A. R. Subramaniam, A. Furusaki, I. A. Gruzberg, and A. W. W. Ludwig, Phys. Rev. B **82**, 035309 (2010).
[45] M. Amado, A. V. Malyshev, A. Sedrakyan, and F. Domínguez-Adame, Phys. Rev. Lett. **107**, 066402 (2011).
[46] H. Obuse, I. A. Gruzberg, and F. Evers, Phys. Rev. Lett. **109**, 206804 (2012).
[47] K. Slevin and T. Ohtsuki, Int. J. Mod. Phys. Conf. Ser. **11**, 60 (2012).
[48] W. Nuding, A. Klümper, and A. Sedrakyan, Phys. Rev. B **91**, 115107 (2015).
[49] J. P. Dahlhaus, J. M. Edge, J. Tworzydło, and C. W. J. Beenakker, Phys. Rev. B **84**, 115133 (2011).
[50] I. C. Fulga, F. Hassler, A. R. Akhmerov, and C. W. J. Beenakker, Phys. Rev. B **84**, 245447 (2011).
[51] D. G. Polyakov and B. I. Shklovskii, Phys. Rev. Lett. **70**, 3796 (1993).
[52] D. G. Polyakov and B. I. Shklovskii, Phys. Rev. B **48**, 11167 (1993).
[53] A. M. M. Pruisken and M. A. Baranov, EPL (Europhysics Letters) **31**, 543 (1995).
[54] D.-H. Lee and Z. Wang, Phys. Rev. Lett. **76**, 4014 (1996).
[55] Z. Wang, M. P. A. Fisher, S. M. Girvin, and J. T. Chalker, Phys. Rev. B **61**, 8326 (2000).
[56] A. M. M. Pruisken and I. S. Burmistrov, Ann. Phys. **322**, 1265 (2007).
[57] A. M. M. Pruisken and I. S. Burmistrov, JETP Letters **87**, 220 (2008).
[58] I. S. Burmistrov, S. Bera, F. Evers, I. V. Gornyi, and A. D. Mirlin, Ann. Phys. **326**, 1457 (2011).
[59] V. G. Knizhnik, A. M. Polyakov, and A. B. Zamolodchikov, Mod. Phys. Lett. **A3**, 819 (1988).
[60] F. David, Mod. Phys. Lett. **A3**, 1651 (1988).
[61] J. Distler and H. Kawai, Nucl. Phys. **B321**, 509 (1989).
[62] V. A. Kazakov, Nucl. Phys. B Proc. Supp. **4**, 93 (1988).
[63] V. A. Kazakov and A. A. Migdal, Nucl. Phys. B **311**, 171 (1988).
[64] V. A. Kazakov, Mod. Phys. Lett. **A4**, 1691 (1989).
[65] B. Duplantier and I. K. Kostov, Nucl. Phys. B **340**, 491 (1990).
[66] M. R. Zirnbauer, J. Math. Phys. **37**, 4986 (1996).
[67] A. Altland and M. R. Zirnbauer, Phys. Rev. B **55**, 1142 (1997).
[68] G. 't Hooft, Nucl. Phys. **B72**, 461 (1974).
[69] E. Brezin, C. Itzykson, G. Parisi, and J. B. Zuber, Comm. Math. Phys. **59**, 35 (1978).
[70] R. Klesse and M. Metzler, Europhys. Lett. **32**, 229 (1995).
[71] M. Janssen, M. Metzler, and M. R. Zirnbauer, Phys. Rev. B **59**, 15836 (1999).
[72] J. Cardy, Comm. Math. Phys. **258**, 87 (2005).
[73] A. R. Kavalov and A. G. Sedrakyan, Nucl. Phys. B **285**, 264 (1987).
[74] A. Sedrakyan, Nucl. Phys. B **554**, 514 (1999).
[75] A. Sedrakyan, in *Statistical Field Theories*, NATO Science Series, Vol. 73, edited by A. Cappelli and G. Mussardo (Springer Netherlands, 2002) pp. 67–78.
[76] A. Sedrakyan, Phys. Rev. B **68**, 235329 (2003).
[77] S. Khachatryan, R. Schrader, and A. Sedrakyan, J. Phys. A **42**, 304019 (2009).
[78] S. Khachatryan, A. Sedrakyan, and P. Sorba, Nucl. Phys. B **825**, 444 (2010).
[79] M. Nakahara, *Geometry, topology, and physics* (Institute of Physics Pub, Bristol Philadelphia, 2003).
[80] A. M. Polyakov, Phys. Lett. B **103**, 207 (1981).
[81] W. Janke, D. A. Johnston, and M. Weigel, Cond. Mat. Phys. **9**, 263 (2006).
[82] A. A. Belavin, A. M. Polyakov, and A. B. Zamolodchikov, Nucl. Phys. **B241**, 333 (1984).
[83] V. I. Oseledec, Trudy Moskov. Mat. Obšč. **19**, 179 (1968).
[84] V. Tutubalin, Theory Probab. Appl. **10**, 15 (1965).
[85] F. Evers, A. Mildenberger, and A. D. Mirlin, Phys. Rev. Lett. **101**, 116803 (2008).
[86] H. Obuse, A. R. Subramaniam, A. Furusaki, I. A. Gruzberg, and A. W. W. Ludwig, Phys. Rev. Lett. **101**, 116802 (2008).
[87] V. Kagalovsky, B. Horovitz, Y. Avishai, and J. T. Chalker, Phys. Rev. Lett. **82**, 3516 (1999).
[88] T. Senthil, J. B. Marston, and M. P. A. Fisher, Phys. Rev. B **60**, 4245 (1999).
[89] T. Senthil and M. P. A. Fisher, Phys. Rev. B **61**, 9690 (2000).
[90] I. A. Gruzberg, A. W. W. Ludwig, and N. Read, Phys. Rev. Lett. **82**, 4524 (1999).
[91] E. J. Beamond, J. Cardy, and J. T. Chalker, Phys. Rev. B **65**, 214301 (2002).
[92] A. D. Mirlin, F. Evers, and A. Mildenberger, J. Phys. A **36**, 3255 (2003).
[93] J. Cardy, Phys. Rev. Lett. **84**, 3507 (2000).

[94] A. R. Subramaniam, I. A. Gruzberg, A. W. W. Ludwig, F. Evers, A. Mildenberger, and A. D. Mirlin, Phys. Rev. Lett. **96**, 126802 (2006).
[95] A. R. Subramaniam, I. A. Gruzberg, and A. W. W. Ludwig, Phys. Rev. B **78**, 245105 (2008).
[96] R. Bondesan, I. A. Gruzberg, J. L. Jacobsen, H. Obuse, and H. Saleur, Phys. Rev. Lett. **108**, 126801 (2012).
[97] S. Bhardwaj, I. A. Gruzberg, and V. Kagalovsky, Phys. Rev. B **91**, 035435 (2015).
[98] S. Cho and M. P. A. Fisher, Phys. Rev. B **55**, 1025 (1997).
[99] J. T. Chalker, N. Read, V. Kagalovsky, B. Horovitz, Y. Avishai, and A. W. Ludwig, Phys. Rev. B **65**, 012506 (2002).
[100] F. Merz and J. T. Chalker, Phys. Rev. B **65**, 054425 (2002).
[101] A. Mildenberger, F. Evers, A. D. Mirlin, and J. T. Chalker, Phys. Rev. B **75**, 245321 (2007).
[102] M. Bocquet, D. Serban, and M. R. Zirnbauer, Nucl. Phys. B **578**, 628 (2000).
[103] H. A. Fertig and B. I. Halperin, Phys. Rev. B **36**, 7969 (1987).
[104] D.-H. Lee, Z. Wang, and S. Kivelson, Phys. Rev. Lett. **70**, 4130 (1993).
[105] F. Evers and W. Brenig, Phys. Rev. B **57**, 1805 (1998).
[106] H. Akaike, IEEE Trans. Automat. Control **19**, 716 (1974).
[107] K. P. Burnham and D. R. Anderson, *Model Selection and Multimodel Inference*, 2nd ed. (Springer-Verlag New York, 2002).